Korean J. Chem. Eng., 34(6), 1786-1792 (2017)
DOI: 10.1007/s11814-017-0065-6

pISSN: 0256-1115
eISSN: 1975-7220

V_2O_5-TiO_2 heterostructural semiconductors: Synthesis and photocatalytic elimination of organic contaminant

Meltem Isleyen, Eda Sinirtas Ilkme, and Gulin Selda Pozan Soylu†

Chemical Engineering Department, Faculty of Engineering, Istanbul University Avcilar, 34320, Istanbul, Turkey
(*Received 25 January 2017 • accepted 7 March 2017*)

Abstract−V_2O_5-TiO_2 binary oxide catalysts were successfully prepared with different wt% V_2O_5 loading by solid state mechanical mixing (SSDMMix), and these nanocomposites were modified with hexadecyltrimethylammonium bromide (HTAB) and cetyl trimethylammonium bromide (CTAB) and polyvinyl alcohol (PVA) as surfactant. The resulting catalysts were characterized by X-ray diffraction (XRD), diffuse reflectance spectroscopy (DRS), scanning electron microscopy (SEM), Braun-Emmet-Teller (BET) analysis of surface area techniques. The photocatalytic activities of all samples were evaluated by degradation of 4-chlorophenol (4CP) in aqueous solution under UV irradiation. 50 wt% V_2O_5-TiO_2 photocatalyst exhibited much higher photocatalytic activity than pure V_2O_5, TiO_2 and P-25. The interaction between V_2O_5 and TiO_2 affected the photocatalytic efficiency of binary oxide catalysts. In addition, CTAB and HTAB-assisted samples significantly enhanced the efficiency of $50V_2O_5$-TiO_2 binary oxide catalyst. The highest percentage of 4-chlorophenol degradation (100%) and highest reaction rate (1.69 mg L^{-1} min^{-1}) were obtained in 30 minutes with ($50V_2O_5$-TiO_2)-CTAB catalyst. It is concluded that the addition of surfactant to binary oxide remarkably enhanced the photocatalytic activity by modifying the optical and electronic properties of V_2O_5 and TiO_2.

Keywords: Photocatalysis, 4-Chlorophenol, V_2O_5-TiO_2, UV Irradiation, Characterization

INTRODUCTION

With rapid industrialization, chemical pollutants, such as dyes, sulfates and toxic compounds, are dumped into rivers and are polluting soil and water. Water pollution by organic and inorganic contaminants is of immense public concern. A typical group of organic contaminants is the phenols, and its derivatives (such as 4-chlorophenol) are some of the most refractory contaminants, which may occur in the environment due to its widespread use in agriculture, petrochemical, textile, paint, plastic, production processes of pesticides and dyes.

These pollutants affecting the environment are particularly serious in developing countries. Moreover, there is a continuously growing problem due to the rising population and increasing demands for water sources. More and more attention is being paid to environmental problems such as organic pollutants and toxic water pollutants produced by some industries are harmful to human health and ecological environment. Conventional wastewater treatment methods like chemical precipitation, activated carbon adsorption and ion-exchange processes are usually effective in the removal of these compounds in wastewater. The high cost of activated carbon, solvent extraction and oxidation treatments has stimulated interest to use cheaper raw materials [1]. Photocatalytic treatment of organic compounds in wastewater using semiconductors has proven to be a promising green technology for environmental purification.

In this field, TiO_2-based photocatalysts have attracted continuously increasing attention because of the excellent properties such as high light-conversion efficiency, chemical stability, nontoxic nature, low cost, and so on [2-7]. However, a disadvantage of the use of TiO_2 as a photocatalyst is due to its relatively large band gap (Eg=3.2 eV for anatase phase), and low photo quantum efficiency.

Various methods are documented to improve photocatalytic efficiency of TiO_2 [8]. A considerable enhancement in the photocatalytic efficiency of TiO_2 under visible light has been obtained by coupling low band gap semiconductors with TiO_2 [9]. As an important transition metal-oxide semiconductor, V_2O_5 has relatively low band-gap energy (about 2.3 eV), which can provide a capability [10,11]. V_2O_5 is the most stable form in the vanadium oxide family, which allows a wide range of practical applications such as electrochromic devices, cathodic electrodes for lithium batteries, gas sensors and so on [12,13].

This makes V_2O_5-TiO_2 system an effective catalytic material for photocatalytic application. Among its interesting properties and possible applications, the photocatalytic action of V_2O_5 makes it a promising candidate for the degradation of organic pollutants such as hydrocarbons. Fei et al. synthesized hollow V_2O_5 microspheres by solvo-thermal route, exhibiting excellent photoactivity for degradation of rhodamine B (RhB) under UV light [14].

We prepared V_2O_5-TiO_2 binary oxide by mechanical solid state dispersion method (SSDMMix) and investigated under UV irradiation for 4 chlorophenol degradation. The aim of this study was to investigate amounts of V_2O_5, and surface additives on crystal structure, morphology and spectroscopic properties of V_2O_5-TiO_2 binary oxide catalysts. Catalysts were characterized by XRD, DRS, FT-IR, SEM as well to explain the relationship between the structure of the catalysts and photocatalytic activities.

†To whom correspondence should be addressed.
E-mail: gpozan@istanbul.edu.tr

EXPERIMENTAL

1. Materials

Starting materials for catalyst preparation were V_2O_5 (Vanadium (V)-oxide, MERCK), TiO_2 (Aeroxide), hexadecyltrimethylammonium bromide (HTAB), cetyl trimethylammonium bromide (CTAB), polyvinyl alcohol (PVA)ethanol (absolute), titanium tetrachloride (≥99 %), carbon tetrachloride (Merck). The organic compounds used in the photocatalytic experiments were 4-chlorophenol, phenol, hydroquinone and catechol were purchased from the Fluka Company. Deionized (D.I.) water was used for the preparation of all the catalysts as well as to dilute the 4-chlorophenol solution. Mobile phase for HPLC analysis was prepared with methanol (HPLC grade, Fluka Company).

2. Catalyst Preparation

Pure TiO_2 was prepared by sol-gel method. 1.5 mL $TiCl_4$ was slowly added dropwise into 15 mL ethanol solution at room temperature. A large amount of HCl gas was exhausted during the mixing process. Then, a light-yellow solution was obtained and gelatinized for several days to form sol-gel. Finally, the gel was dried in the oven at 105 °C for one day, ground into fine powder, and calcined at 600 °C for 4 h.

3. Synthesis of V_2O_5-TiO_2 Binary Oxide Photocatalyst

V_2O_5-TiO_2 binary oxide catalysts were prepared by mechanical solid state dispersion method. In this method, V_2O_5 and TiO_2 samples were ground at a constant vibration rate of 300 rpm for 10 hours in a Retsch MM 200 vibrant-ball mill by milling ball in milling container. Then it was dried at 110 °C for 90 min, and calcined in air at 450 °C for 6 h and ball milled. V_2O_5 loading of the catalysts was nominally 10, 30, 50 and 90 wt% and reported as the weight percentage. For instance, 10 V_2O_5-TiO_2 means that the catalyst contained nominally 10% V_2O_5 by weight.

In addition, surfactant-assisted V_2O_5-TiO_2 catalysts were prepared by solid state dispersion method. V_2O_5-TiO_2 binary oxide and surfactant (CTAB, HTAB or PVA) mixed in weight rate of 1 : 1. The resultant catalyst was dried at 110 °C for 90 min, and it was heated at 150 °C in air for 5 h with a heating rate of 10 °C/min and ball milled.

4. Catalyst Characterization

The BET surface areas of the samples were determined by nitrogen adsorption-desorption isotherm measurement at 77 K. The samples were degassed at 200 °C prior to the actual measurements.

Powder X-ray diffractions of samples were obtained using a Rigaku D/Max-2200 diffractometer with the CuKα (λ=1.540) radiation. Samples were scanned from 10 to 90 at a rate of 2°/min (in 2θ). The sizes of the crystalline domains were calculated by using the Scherrer equation, t=Cλ/BcosΘ, where is the X-ray wavelength (A°), B is the full width at half maximum, Θ is Bragg angle, C is a factor depending on crystallite shape (taken to be one), and t is the crystallite size (A°).

The morphology and size distribution of the photocatalysts were recorded by scanning electron microscopy (JEOL/JSM-6335F).

The surface OH groups of the photocatalysts were determined by Fourier transform infrared spectra using KBr in the form of pellets (PerkinElmer Precisely Spectrum One). All measurements were at 4 cm^{-1} resolution and 100 scans.

UV-vis diffuse reflectance spectra of the samples were obtained on an UV-vis spectrophotometer (Shimadzu UV-3600) using $BaSO_4$ as the reference.

5. Evaluation of Photocatalytic Activity

Photocatalytic activity of the V_2O_5-TiO_2 powders was evaluated by degradation of 4-chlorophenol in a quartz batch-photoreactor of cylindrical shape. In a typical experiment, 100 mg catalyst was dispersed in 50 mL 4-chlorophenol solution of initial concentration 25 mg/L and neutral pH under magnetic stirring. To compare the light sources, photocatalytic activity of catalyst which has the best photocatalytic activity was measured under UV and visible light irradiation. Before illumination, the mixed solution was ultrasonicated for 5 min and magnetically stirred for 1 h in the dark to ensure the establishment of the adsorption-desorption equilibrium between the catalyst and the solution. 0.3 mL of H_2O_2 solution (30 wt%) were added to 50 mL of the phenol-containing aqueous solution. After irradiation, the phenol solution was filtered through a membrane filter (pore size 0.45 mm) and the filtrate was used for TOC measurement with a TOC-V, Shimadzu equipment. The concentration of phenol and products were analyzed by HPLC equipped with C-18 column. The mobile phase used in HPLC was a mixed solvent of methanol and water (60/40, v/v) with a flow rate of 1 mL/min.

To handle the reusability issue of the catalyst, after separating it via centrifugation, the recovered catalyst was used with fresh dye

Table 1. The crystallite sizes, specific surface areas, band gap, morphology of materials and 4-chlorophenol degradation efficiencies over 30 min (%)

Catalyst	Crystallite size		S_{BET} ($m^2\ g^{-1}$)	Band gap (eV)	4-Chlorophenol degradation efficiencies over 30 min (%)	kr ($mg\ L^{-1}\ min^{-1}$)
	V_2O_5	TiO_2 (nm)				
10V_2O_5-TiO_2	36	32	32	2.31	48	0.58
50V_2O_5-TiO_2	38	27	24	2.27	80	0.86
70V_2O_5-TiO_2	39	25	20	2.24	71	0.76
90V_2O_5-TiO_2	42	22	15	2.21	69	0.65
(50V_2O_5-TiO_2)-HTAB	31	42	8	2.24	91	1.01
(50V_2O_5-TiO_2)-CTAB	28	40	12	2.21	100	1.69
(50V_2O_5-TiO_2)-PVA	40	35	5	2.26	39	0.52
V_2O_5	40	-	25	2.35	59	0.62
TiO_2 (syn)	-	43	40	3.12	55	0.60
TiO_2 (Aeroxide)	-	32	50	3.12	48	0.57

solutions. All the experimental parameters were kept constant and the experiments were repeated for five sets of fresh dye solutions.

RESULTS AND DISCUSSION

1. Texture Properties of V_2O_5-TiO_2 Binary Oxide

The actual weight percentages of the oxides (V_2O_5 and TiO_2) in the binary oxide catalysts were obtained by ICP-MS analysis. The calculated wt% of the catalysts and the ICP-MS values were almost similar. Furthermore, ICP-MS values of the two representative catalysts clearly suggest that there may not be any noticeable differences between the calculated values and ICP values for the other weight percentages of V_2O_5 and TiO_2.

1-1. BET Surface Area

The BET surface areas for different catalysts are shown in Table 1. The surface area of V_2O_5 and TiO_2 (Aeroxide) is 25 and 40 $m^2 g^{-1}$, respectively. For the V_2O_5-TiO_2 series, surface areas are decreasing with the increase in V_2O_5 content. This is due to the increasing coverage of surface by the V_2O_5 particle, which prevents the entry of nitrogen probe molecule. According to results, the specific surface area was influenced from different surfactant loading (Table 1). In addition, BET surface area of 50 wt% V_2O_5-TiO_2 was decreased to lower values. This effect may be attributed to the presence of surfactant in the pore mouths of the binary oxide pores and channels.

1-2. X-ray Diffraction Analysis

Fig. 1 shows the XRD patterns of 50 wt% V_2O_5-TiO_2 powders as a function of different synthesis methods and surface active agents. TiO_2 crystallites in V_2O_5-TiO_2 binary oxides which have a tetragonal TiO_2 structure (JCPDS card no 21-1272) and mononoclinic V_2O_5 (JCPDS card no 41-1426) were the major crystalline phases detected on the X-ray diffraction patterns. As shown, the peaks at 25.4, 37.0, 37.9, 38.6, 47.9, 54.0, 55.2, 62.9, 68.9, 70.4, 75.2, 76.2, 83.1 elu-

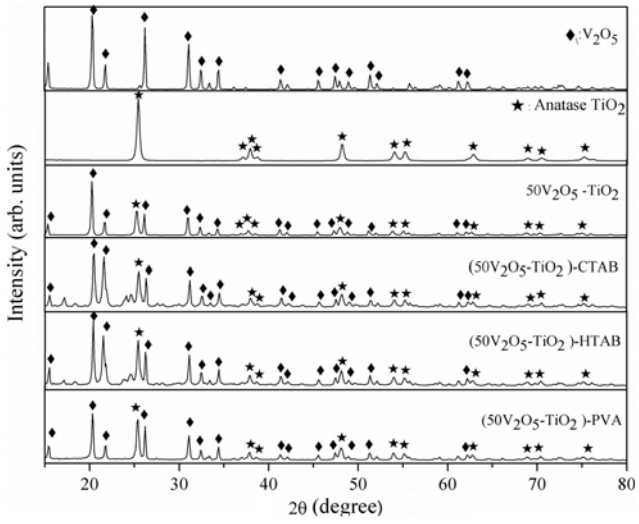

Fig. 1. XRD patterns of V_2O_5, TiO_2, $50V_2O_5$-TiO_2 and surfactant-assisted catalysts.

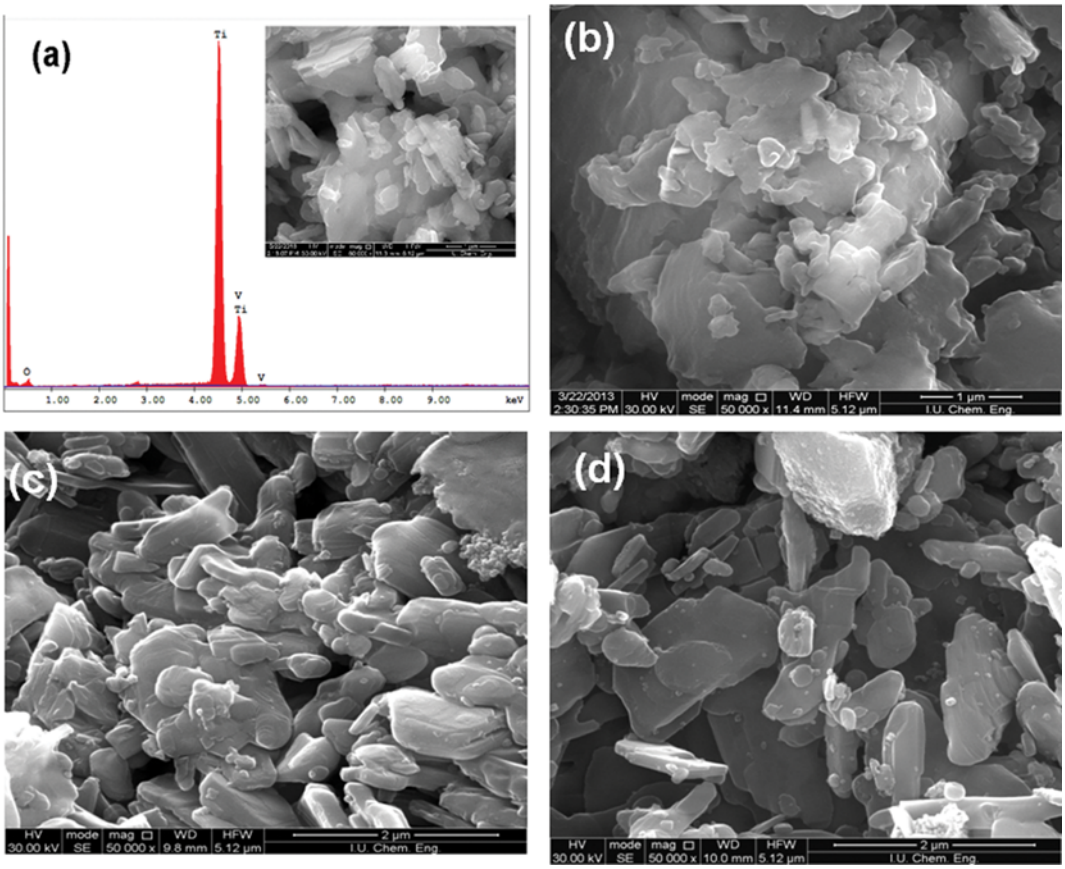

Fig. 2. SEM pattern of (a) $50V_2O_5$-TiO_2, (b) ($50V_2O_5$-TiO_2)-CTAB, (c) ($50V_2O_5$-TiO_2)-HTAB and (d) ($50V_2O_5$-TiO_2)-PVA powders.

cidate the diffractions of the (1 0 1), (1 0 3), (0 0 4), (1 1 2), (0 0 0), (1 0 5), (2 1 1), (2 0 4), (1 1 6), (2 2 0), (2 1 5), (3 0 1) and (2 2 4), respectively, of the pure anatase phase of TiO_2. All the peak positions were in agreement with those of anatase TiO_2 and no peak of brookite or rutile TiO_2 was found in the pattern.

The crystallite grain sizes of the catalysts were calculated according to the Scherrer formula and the results are listed in Table 1.

The diffraction patterns of surfactant-assisted 50 wt% V_2O_5-TiO_2 binary oxides are shown in Fig. 1. Although all samples showed the same morphological arrangements, crystallite size changed with the addition of surfactant. As a result, the V_2O_5 crystalline sizes of samples were evaluated as 40, 31, 28 nm for ($50V_2O_5$-TiO_2)-PVA, ($50V_2O_5$-TiO_2)-HTAB, ($50V_2O_5$-TiO_2)-CTAB, respectively.

This dissimilarity may lead to the differences in their morphology and structure [15]. The crystallite size of ($50V_2O_5$-TiO_2)-CTAB catalyst was smaller than that of the V_2O_5 and TiO_2 catalysts; this contraction may be due to the addition of surfactant into the V_2O_5 lattice. Also, the crystallite size decreases with increase in TiO_2 content.

1-3. Scanning Electron Microscopy (SEM)

The SEM images of $50V_2O_5$-TiO_2 and surfactant-assisted V_2O_5-TiO_2 catalysts are shown in Fig. 2. In Fig. 2(a), SEM image of $50V_2O_5$-TiO_2 shows that the sample possesses a mixture of morphologies, including micro-and macro-clusters. Fig. 2(a) shows SEM-EDS image of the $50V_2O_5$-TiO_2 catalyst. In the absence of surfactant there is non-uniform grain structure because of mixed oxides. EDS analysis indicated Ti, V and O on the $50V_2O_5$-TiO_2 surface. The results obtained from SEM-EDS clearly display that the synthesized $50V_2O_5$-TiO_2 consisted of particles. In Fig. 2(b), interaction of particles increased with CTAB surfactant. However, after loading of HTAB and PVA some the rod-like-shaped morphology disappeared. On the other hand, agglomeration of particles can be easily observed with ($50V_2O_5$-TiO_2)-HTAB and ($50V_2O_5$-TiO_2)-PVA catalysts. Due to the van der Waals interaction of surfactant molecules adsorbed on the nanocrystal surfaces and the tendency to minimize the interfacial energy, these nanoparticles would gradually self-assemble into aggregates with a specific morphology [16,17]. In addition, the surfactants are the structure directing agents that could reduce particle size and thus they influence the particle morphology [18].

1-4. UV Diffuse Reflectance Spectroscopy

The optical absorption property of a semiconductor, which is relevant to the electronic structure feature, is recognized as the key factor in determining its photocatalytic activity [16]. The calculated band gap of pure TiO_2 is 3.12, whereas the band gap is lowered to 2.31 eV by the addition of 10 wt% V_2O_5. The band absorptions of the V_2O_5-TiO_2 samples shift to longer wavelengths gradually with the increment of V_2O_5 content.

In addition, band gap value changed with the addition of surfactant. The band gap of $50V_2O_5$-TiO_2 is about 2.27 eV, whereas it is decreased to 2.21 eV by the addition of 1 : 1 (w/w) CTAB. Compared with the V_2O_5-TiO_2, the surfactant-assisted samples exhibit a red-shift of absorption edge and a significant enhancement of light absorption in the visible light region. The red-shift of absorption edge is attributed to the charge-transfer transition between the d electrons of the dopant and the conduction band (or valence band) of TiO_2 [15].

1-5. FT-IR Spectroscopy

Photocatalyst samples were also analyzed by FTIR spectroscopy

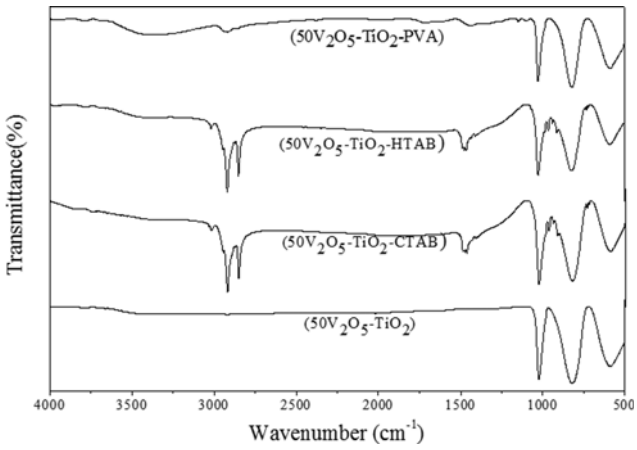

Fig. 3. FT-IR spectra of powders.

(Fig. 3). The bending mode of vibration of Ti-O-Ti observed around 420-650 cm^{-1} confirms the formation of anatase TiO_2. Note that the XRD result of this sample indicated the presence of anatase. The IR spectrum of pure crystalline V_2O_5 shows sharp absorption bands at 1020 and another at 820 cm^{-1} due to V=O stretching and V-O-V deformation modes, respectively [19]. The bands at 844 and 580 cm^{-1} are due to O-V-O stretching modes are observed for pure V_2O_5. The presence of bands around 1,000-1,030 cm^{-1} represents the O-V-O stretching vibration and the band around 800-830 cm^{-1} due to Ti-O-V linkage [20] was observed for V_2O_5-TiO_2 and surfactant doped V_2O_5-TiO_2 binary oxides. Furthermore, the sharp bands at about 2,850, 2,918 and 1,474 cm^{-1} are assigned to the C-H and C=C stretches. The absorption bands at 2,918 and 2,850 cm^{-1} are due to the C-H asymmetric and symmetric stretching vibrations of CTAB and HTAB, respectively [21]. As a result, the higher catalytic activity of supported V_2O_5-TiO_2 catalysts originated from a higher concentration of these C-H groups of pure V_2O_5-TiO_2.

2. Photocatalytic Activity

The photocatalytic activities of the as-fabricated samples were measured on the degradation of 4-chlorophenol in aqueous solution in the presence of small amount of H_2O_2 under UV-A irradiation.

In general, the diffusion rate of adsorbed reactive species on the surface is faster than the photocatalytic reaction rate. Therefore, the photocatalytic reaction is the rate control step. The Langmuir-Hinshelwood model is usually used to describe the kinetics of photocatalytic reactions of aquatic organics [22,23]. It basically relates the degradation rate (r) and the concentration of organic compound (C) which is expressed as follows:

$$r = -\frac{dC}{dt} = \frac{k_r K_{ads} C}{1 + K_{ads} C}$$

where k_r is the Langmuir-Hinshelwood reaction rate constant (mg L^{-1} min^{-1}) and K is the Langmuir adsorption constant (L mg^{-1}).

The photocatalytic degradation performance for V_2O_5, TiO_2, and V_2O_5-TiO_2 binary oxide catalysts prepared was monitored for the oxidative degradation of 4-chlorophenol, and the results are shown in Fig. 4.

The performance of V_2O_5-TiO_2 catalysts with varying V_2O_5 load-

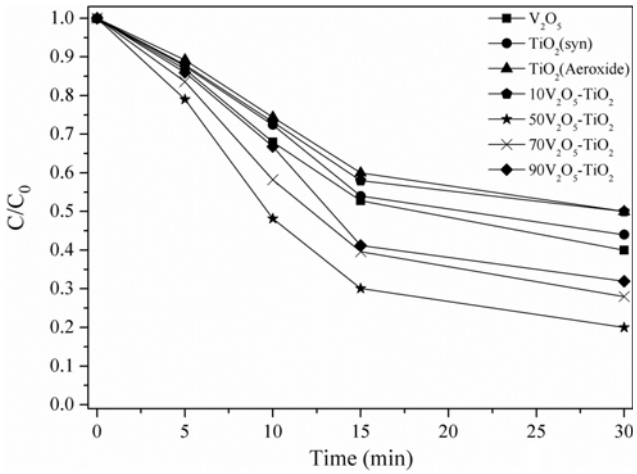

Fig. 4. Time course of the adsorption of 4-chlorophenol by the different catalysts.

ings was also studied. When a lower amount of V_2O_5 (10-50 wt%) was loaded to TiO_2, the catalytic activity of the binary oxide catalysts gradually increased with an increase in the amount of V_2O_5 loading; however, after 50 wt%, there was a decrease in the reactivity. Also, 4-chlorophenol degradation decreased from 80 to 69% with the 90 wt% V_2O_5 added with TiO_2. In fact, decrease in activity could probably be explained by partial blocking of the active species of TiO_2 due to the formation of larger V_2O_5 particles at higher V_2O_5 loadings. The results showed that surface area and particle size of samples were changed with the loading of V_2O_5. In addition to this result, the tendency of V_2O_5 to form larger particles on the surface also caused to lower the conversion of 4-chlorophenol.

The photocatalytic degradation performance for these catalysts was monitored for the oxidative degradation of phenol; the results are shown in Table 1. 55 and 59% degradation of 4-chlorophenol were achieved with the pure TiO_2 and V_2O_5 catalysts under UV light irradiation for 30 minutes. The 50 wt% V_2O_5 showed the highest percentage of phenol degradation (100%); however, after that weight percentage, there was noticeable change in the reactivity; and the value remained the same with further loadings of V_2O_5 (Table 1). Also, 4-chlorophenol degradation decreased from 100 to 48% with the 10 wt% V_2O_5 mixed with TiO_2.

Su et al. described that all the V_2O_5/TiO_2 nanoheterostructures exhibited more prominent photocatalytic activity than that of pure TiO_2 nanopowders. At least 62% 4cp molecules were decomposed using the V_2O_5-TiO_2 nanoheterostructures as photocatalysts after 30 min of UV-A irradiation, but only 55% 4-chlorophenol molecules were decomposed using pure TiO_2 nanopowders as the photocatalysts [24].

The degradation rate of pollutant is influenced by the active site and the photoabsorption of the catalyst used. Adequate loading of V_2O_5 to TiO_2 catalyst increases the generation rate of electron/hole pairs for enhancing the degradation of pollutant. However, addition of a high dose of V_2O_5 decreases the light penetration by the photocatalyst suspension and reduces the degradation rate.

The activity results revealed that V_2O_5-TiO_2 binary oxides exhibited mixed monoclinic V_2O_5 and anatase phase of TiO_2. The photocatalytic activity is influenced by the amount of the monoclinic V_2O_5 phase. Clearly, the activity varies in parallel with the amount of monoclinic phase. The catalytic activity of the binary oxide catalysts gradually increased with an increase in the amount of monoclinic phase for a lower amount of V_2O_5 (10-50 wt%). However, after 50 wt%, there was a decrease in the reactivity in parallel with the amount of monoclinic phase for a higher amount of V_2O_5 (70-90 wt%). This result may show that the anatase phase of TiO_2 may not improve the photodegradation. Based on the XRD patterns of catalysts, the presence of monoclinic phase of V_2O_5 is more effective in photodegradation reactions.

The activity of the photocatalyst is influenced by its crystallinity as well as by surface area, crystal size, synthesis method, band gap, crystal phase and surface OH group. According to the activity results, the surface area, particle size and surface OH groups were not the only contribution in high reactivity for the degradation of phenol. The reaction with the binary oxide catalysts is more important beside the surface area, particle size and surface OH groups. The optimum photodegradation activity was seen at 50 wt% V_2O_5-TiO_2. Our XRD observations clearly show that V is in interaction with the Ti.

Neppolian et al. expressed that electron injection was shown to be the major factor in the high activity of the binary oxide catalysts along with other physicochemical characteristics. The transfer of electrons from ZrO_2 to TiO_2 was seen to be the main phenomenon in the binary oxide catalyst through chemical interactions between ZrO_2 and TiO_2 in the form of the Ti-O-Zr-bond [25].

In addition, Wu et al., described the formation of a mutual chemical interaction between the pure oxides when they are coprecipitated together (-Ti-O-Zr-), leading to a profound effect on the photocatalytic properties [26]. In our study, 50 wt% V_2O_5-TiO_2 compared to nano-TiO_2 (synthesized) and Aeroxide-P25 TiO_2 exhibited superior photocatalytic activity. Although the decrease in surface area of $50V_2O_5$-TiO_2 catalyst was comparable even lower than TiO_2 and P-25, it showed high activity. However, the changes in surface areas were not as drastic as the changes in catalytic activities; hence, the activity comparisons were due to the active species on the surface. Some researchers have found that the synthesized novel catalysts have a higher photocatalytic activity than the Degussa-P25 [27,28]. Xu et al. (1995) investigated the photocatalytic activity of titanium oxide supported on ZSM5, zeolite A, silica, and alumina using the photooxidation of 4-chlorophenol and acetophenone [29]. The photocatalytic activity of TiO_2/ZSM5 was higher than TiO_2 powder prepared and Degussa P25.

Fig. 5(a) shows the UV light-induced photocatalytic activity of the samples supported with various surfactants after exposure to UV-A light. It can be clearly realized that the photocatalytic performance over the as-prepared catalysts within 30 min of reaction decreased according to the sequence of ($50V_2O_5$-TiO_2)-CTAB (ca. 100%)>($50V_2O_5$-TiO_2)-HTAB (ca. 87%)>($50V_2O_5$-TiO_2) (ca. 81%)> ($50V_2O_5$-TiO_2)-PVA (ca. 62%). Obviously, the (V_2O_5-TiO_2)-CTAB sample can be completely degraded in 30 min among these samples (Table 1). However, 37% degradation of 4-chlorophenol were achieved with the (V_2O_5-TiO_2)-PVA catalyst for 30 minutes. In fact, a decrease in activity could probably be explained by partial blocking of the active species of V_2O_5-TiO_2 binary oxide due to the larger

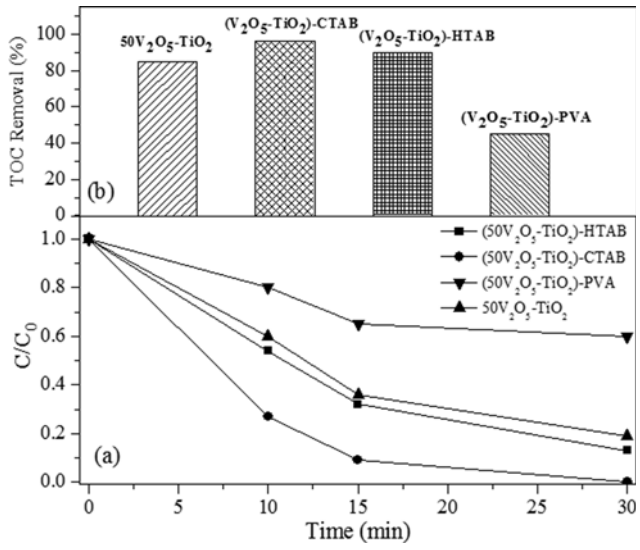

Fig. 5. (a) Time course of the adsorption of 4-chlorophenol by surfactant-assisted catalysts (b) The impact of surfactant on TOC removal in the 4-chlorophenol degradation.

PVA particles. The results showed that surface area and particle size of samples were changed with the loading of surfactant.

In addition, the reusability of the ($50V_2O_5$-TiO_2)-CTAB catalyst was studied on fresh dye samples (5 trials). ($50V_2O_5$-TiO_2)-CTAB, when used for the first time, could degrade 100% 4-chlorophenol, with a small change (to 95.42%) in the efficiency when used for five times. This decrease in the efficiency for ($50V_2O_5$-TiO_2)-CTAB catalyst resulted probably from the photocorrosion effect.

Fig. 5(b) presents the TOC removal results on the photocatalytic degradation of 4-chlorophenol with $50V_2O_5$-TiO_2, ($50V_2O_5$-TiO_2)-CTAB, ($50V_2O_5$-TiO_2)-HTAB and ($50V_2O_5$-TiO_2)-PVA. 25 ppm 4-chlorophenol can be completely degraded in 30 min by ($50V_2O_5$-TiO_2)-CTAB sample and 96% TOC removal can be achieved in 30 min. This result emphasizes the achievement of the total mineralization.

HPLC analysis performed during the photocatalytic degradation of 4-chlorophenol. Hydroquinone (HQ; 4-hydroxyphenol), Catechol (CT; 2-hydroxyphenol), phenol (Ph), hydroxyhydroquione (HHQ) and 2-chlorophenol (2-CP) were detected as intermediates. Also, ring-opening products are supposed to be short chain acids, such as, acetic acid, maleic acid, oxalic acid [30]; they were identified by GC-MS analysis.

Concentration profiles for 4CP, phenol, catechol and the other products obtained during the photocatalytic oxidation reaction using pure and CTAB-assisted $50V_2O_5$-TiO_2 binary oxide catalysts are shown in Fig. 6. According to HPLC results, CT and Ph were detected as main intermediate by using $50V_2O_5$-TiO_2 (Fig. 6(a)). In addition to these products, ring-opening products (others) were also detected in very low concentration. Moreover, with CTAB addition to pure catalyst, the concentration of CT and Ph were detected in very low concentration (Fig. 6(b)).

Besides, the concentration of ring-opening products was considerably higher than the concentration of intermediate products by using CTAB. These intermediates undergo further photocatalytic oxidation to ring cleavage to yield carboxylic acids and aldehydes, which give CO_2 and H_2O due to decarboxylation.

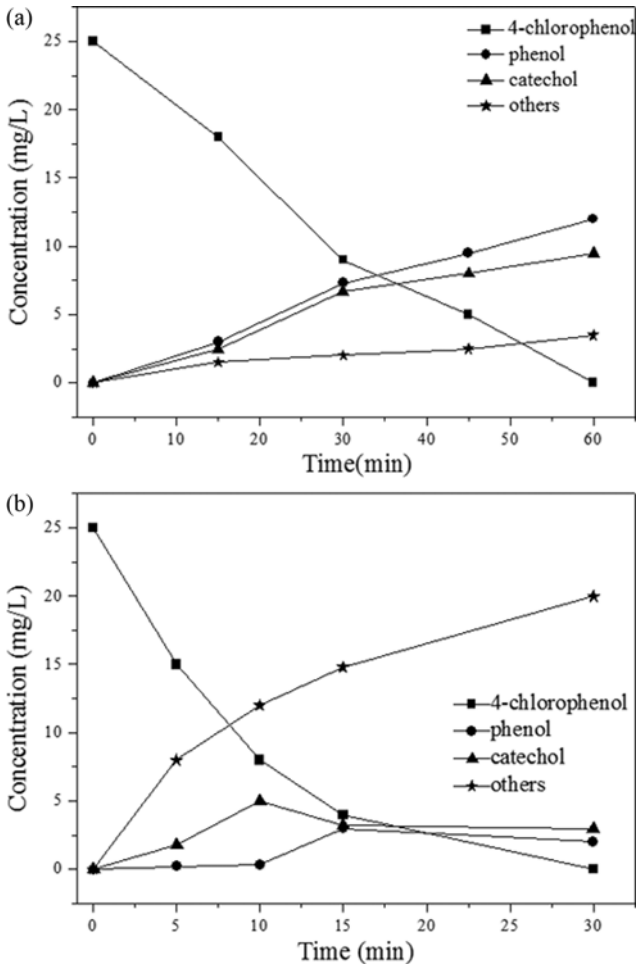

Fig. 6. Concentration profiles for intermediates obtained during the photocatalytic oxidation reaction using (a) $50V_2O_5$-TiO_2 (b) ($50V_2O_5$-TiO_2)-CTAB.

CONCLUSION

V_2O_5-TiO_2 binary oxide catalysts with different weight ratio were prepared by solid state dispersion method and were successfully used in the photocatalytic degradation of 4-chloropenol under UV irradiation. The photocatalytic efficiency was significantly enhanced by V_2O_5-TiO_2 binary oxides.

The photocatalytic efficiency decreases with V_2O_5 content increase up to the optimum V_2O_5 doping concentration of 50% (w/w). For higher V_2O_5 content, larger V_2O_5 particles were observed on TiO_2 (synthesized) surface. Also, the catalytic activity of $50V_2O_5$-TiO_2 was found to be higher than the standard Aeroxil-P25 photocatalyst.

The influence of surfactant loading on the photocatalytic activity of the V_2O_5-TiO_2 samples was investigated. The results showed that surfactant of CTAB, HTAB, and PVA strongly affected the particle morphology and crystalline of structure of powder. ($50V_2O_5$-TiO_2)-CTAB catalyst showed enhanced photocatalytic activity in the degradation of 4-chlorophenol. The highest percentage of 4-

chlorophenol degradation (100%) and highest reaction rate (1.69 mg L^{-1} min^{-1}) were obtained in 30 minutes on ($50V_2O_5$-TiO_2)-CTAB catalyst. The incorporation of CTAB in binary oxide catalyst led to small grain size (28 nm) and low band gap values (2.21 eV).

Finally, the structural and optical properties of V_2O_5-TiO_2 binary oxide catalyst led to a profound positive effect on the photocatalytic activity for degradation of 4-chlorophenol.

ACKNOWLEDGEMENT

This work was supported by The Scientific and Technological Research Council of Turkey (TUBITAK) for the financial support within the research project 111M210 [2011-2013] and Scientific Research Projects Coordination Unit of Istanbul University within the Project number 29248.

REFERENCES

1. R. C. Wang, D. J. Ren, S. Q. Xia, Y. L. Zhang and J. F. Zhao, *J. Hazard. Mater.*, **169**, 926 (2009).
2. M. R. Hoffmann, S. T. Martin, W. Choi and D. W. Bahnmann, *Chem. Rev.*, **95**, 69 (1995).
3. A. L. Linsebigler, G. Lu and J. T. Yates, *Chem. Rev.*, **95**, 735 (1995).
4. R. Asahi, T. Morikawa, T. Ohwaki, K. Aoki and Y. Taga, *Science*, **293**, 269 (2001).
5. J. G. Yu, H. G. Yu, B. Cheng, X. J. Zhao, J. C. Yu and W. K. Ho, *J. Phys. Chem.*, **107**, 13871 (2003).
6. A. Kudo and Y. Miseki, *Chem. Soc. Rev.*, **38**, 253 (2009).
7. Y. Kuwahara and H. Yamashita, *J. Mater. Chem.*, **21**, 2407 (2011).
8. C. Karunakaran, P. Gomathisankar and G. Manikandan, *Mater. Chem. Phys.*, **123**, 585 (2010).
9. D. Jiang, Y. Xu, B. Hou, D. Wu and Y. Sun, *J. Sol. State Chem.*, **180**, 1787 (2007).
10. R. Akbarzadeh, S. B. Umbarkar, R. S. Sonawane, S. Takle and M. K. Dongare, *Appl. Catal. A.*, **374**, 103 (2010).
11. Y. Wang, Y. R. Su, L. Qiao, L. X. Liu, Q. Su and C. Q. Zhu, *Nanotechnology*, **22**, 22 (2011).
12. J. F. Liu, X. Wang, Q. Peng and Y. D. Li, *Adv. Mater.*, **17**, 764 (2005).
13. K. Lee, Y. Wang and G. Z. Cao, *J. Phys. Chem. B*, **109**, 16700 (2005).
14. H. L. Fei, H. J. Zhou, J. G. Wang, P. C. Sun, D. T. Ding and T. H. Chen, *Solid State Sci.*, **10**, 102 (2009).
15. W. Choi, A. Termin and M. R. Hoffmann, *J. Phys. Chem.*, **98**, 13669 (1994).
16. F. Bai, D. S. Wang, Z. Y. Huo, W. Chen, L. P. Liu, X. Liang, C. Chen, X. Wang, Q. Peng and Y. D. Li, *Angew. Chem. Int. Ed.*, **46**, 6650 (2007).
17. Q. Peng, Y. J. Dong and Y. D. Li, *Angew. Chem. Int. Ed.*, **42**, 3027 (2003).
18. V. D. Nithya, R. K. Selvan, C. Sanjeeviraja, D. M. Radheep and S. Arumugam, *Mater. Res. Bull.*, **46**, 1654 (2011).
19. G. C. Bond and S. F. Tahir, *Appl. Catal.*, **71**, 1 (1991).
20. M. Kanna and S. Wongnawa, *Mater. Chem. Phys.*, **110**, 166 (2008).
21. G. M. Chen, S. H. Liu, S. J. Chen and Z. N. Qi, *Macromol. Chem. Phys.*, **202**, 189 (2001).
22. S. Lathasree, A. N. Rao, B. SivaSankar, V. Sadasivam and K. Rengaraj, *J. Mol. Catal. A: Chem.*, **223**, 101 (2004).
23. T. Yonar, K. Kestioglu and N. Azbar, *Appl. Catal. B: Environ.*, **67**, 223 (2006).
24. Y. Wang, Y. R. Su, L. Qiao, Q. Su, C. Q. Zhu and X. Q. Liu, *Nanotechnology*, **22**, 225702 (2011).
25. B. Neppolian, Q. Wang, H. Yamashita and H. Choi, *Appl. Catal. A.*, **333**, 264 (2007).
26. J. C. Wu, C. S. Chung, C. L. Ay and I. Wang, *J. Catal.*, **87**, 98 (1984).
27. L. Zhang, T. Kanki, S. Norikai and A. Toyada, *Solar Energy*, **70**, 331 (2001).
28. D. Vione, C. Minero, V. Maurino, M. E. Carlotti, T. Picatonotto and E. Pelizzetti, *Appl. Catal. B: Environ.*, **58**, 79 (2005).
29. Y. Xu and C. H. Langford, *J. Phys. Chem.*, **99**, 11501 (1995).
30. B. Tryba, A. W. Morawski, M. Inagaki and M. Toyoda, *Appl. Catal. B: Environ.*, **63**, 215 (2006).